An investigation on the behavior of the torch flame in the LBGE combustion process

Abdelhameed, Elsayed
Interdisciplinary Graduate School of Engineering Sciences, Kyushu University

Tashima, Hiroshi
Interdisciplinary Graduate School of Engineering Sciences, Kyushu University

https://doi.org/10.5109/5909093

出版情報：Proceedings of International Exchange and Innovation Conference on Engineering & Sciences (IEICES). 8, pp.207-214, 2022-10-20. Interdisciplinary Graduate School of Engineering Sciences, Kyushu University
バージョン：

Proceedings of the 8th International Exchange and Innovation Conference on Engineering & Sciences (IEICES 2022)

An investigation on the behavior of the torch flame in the LBGE combustion process

Elsayed Abdelhameed[1,2*] and Hiroshi Tashima[1]
[1] Interdisciplinary Graduate School of Engineering Sciences, Kyushu University, Japan
[2] Faculty of Engineering, Kafrelsheikh University, Kafrelsheikh 33511, Egypt
*Corresponding Author email: email: abdelhameed.elsayed.203@s.kyushu-u.ac.jp

Abstract: *Fuel conversion from heavy fuel oil (HFO) to LNG-based fuel, of which the main component is methane, is considered a suitable and practical solution. Most LBGEs adopt the pre-chamber (PC) configuration that can promote premixture combustion in the Main Combustion Chamber (MC) thanks to torch flame ejection from the orifice holes of the PC. However, the PC is sometimes specified as a starting point of the pre-ignition phenomenon that is a significant obstacle for Lean Burn Gas Engines (LBGEs) to improve their thermal efficiency. Too strong ejection may result in a misfire of the premixture MC and a considerable cyclic variation of the MC combustion. In this study, detailed observation of the combustion process was done in LBGE-simulating devices focusing on the ejection behaviors of the torch flame to clarify the source of the abnormal combustion and the cyclic variation of combustion processes.*

Keywords: Combustion; Gas engines; Lean burn; Methane; Pre-chamber.

1. INTRODUCTION

The temperature of our planet "Earth" could rise by 2°C (3.6°F) by 2050; at present, greenhouse gas (GHG) emission rates, which the United Nations' Intergovernmental Panel on Climate Change (IPCC) states, is the upper limit to prevent "dangerous" levels [1]. Burning fossil fuel for our vehicles, trucks, ships, trains, and planes is the primary source of greenhouse gas emissions from transportation [2,3]. From 1990 to 2020, the GHG emissions from the transportation sector grew by 92% [4]. As of 2020, transportation produced almost 27% of all global warming-related greenhouse gas emissions. The maritime industry, the backbone of worldwide transportation, provides 80% of the global trade exchange [5].

While the worldwide trade was blooming over the last decades, the ship and tanker manufacturers were striving to lower fuel costs to minimize ship running costs [6]. Marine Heavy Fuel Oil (HFO) is mainly derived from the residue leftover after refining crude oil, providing an economical choice for ship fuel because of its lower price [7]. Meanwhile, The shipping industry emissions reached 2.89% of worldwide anthropogenic CO_2 emissions in 2018, according to the Fourth International Maritime Organization (IMO) GHG Study in 2020 [8,9]. MARPOL Annex VI had advised that the IMO strictly regulated the emissions to minimize NOx emissions by 75% in Tier III. In addition to NOx and SOx, marine fuels are subject to environmental regulations covering GHG. IMO's current agreement on GHG emissions calls for 40% CO_2 emissions per unit of transport volume by 2030, a 50% reduction in overall GHG by 2050, and zero GHG as soon as possible this century, compared to 2008. To fulfill the IMO Tier III NOx emission restrictions, the premixed gas engine has been applied to decrease the emissions by using Natural gas. Also, there have been for replacing a percentage of diesel fuel in the diesel engine with a biodiesel [10,11] fuel or biodiesel with other additives [12,13]. In the heart of the Gas engines, the Lean Burn Gas Engine (LBGE) can produce far fewer emissions thanks to the methane's higher hydrogen to carbon percentage content, reducing GHG by 28% [14]. Natural gas has a low impact on the environment due to its low combustion temperature, its zero content of SOx, and its low levels of NOx emissions [15]. On the other hand, due to its slower flame propagation [16], natural gas usage leads to a longer combustion time for engines [17] and lower thermal conversion efficiency. Due to the methane having a high resistance to knocking, methane has been used in the medium size bore engine, yet the engine can still suffer from knocking because of the end-gas autoignition [18]. Besides the knocking, using the methane could lead to a methane slip and decrease the thermal efficiency.

The lean-burn combustion technique has been applied to decrease the intensity of the knocking in the gas engine, poor ignition, and slower burn-through of the mixture. To perform lean burn combustion, some engines use a pre-chamber to ignite the fuel and then deliver the partially combusted flame into the engine cylinder through several orifices forming a jet flow growing in the main chamber radially with an inclined angle concerning the center of the engine cylinder. This previously propagated jet flow is known as the Torch flame. This torch flame propagation is the ordinary behavior in commercial gas engines. In this type of engine, the two chambers are called the pre-chamber (PC) and the main chamber (MC) [19]. Usually, the pre-chamber volume is around 2% of the main chamber. Zhu et al. [20] comprehensively reviewed the combustion using the pre-chamber as a future low-carbon spark-ignition engine. This study concluded that the piston's movement could mostly control scavenging and filling in the pre-chamber. At the same time, the jets' thermal, chemical, and turbulence effects control the combustion in the main chamber. Controlling the jet penetration in the pre-chamber design is essential to reduce the distance each flame front travels to consume the charge. The orifice diameter is the essential geometrical parameter influencing scavenging, flame quenching, and jet velocity. Talei et al. [21] performed an experimental and numerical study to evaluate the effectiveness of combining the pre-chamber combustion with the EGR system. The results indicated that a 50% in NOx reduction obtained with a slight decrease in CO emissions. The indicated adequate pressure decreased by 3-4%, slightly affecting the engine efficiency. This study concluded that the ideal EGR percentage with the pre-chamber is 10%.

In LBGE, the pre-chamber is applied to increase the combustion stability. From the literature review, some researchers evaluated the performance of the pre-chamber orifices based on engine performance, while others measured the propagation of the ordinary torch flame. The propagated torch flame from the pr-chamber orifices to the main chamber is slightly inclined toward the main chamber center line. In this research, a fuel supply system that can independently control the fuel concentration of the pre-chamber and the main chamber is attached to a constant-volume combustion chamber with the same structure and scale as the standard marine diesel engine. At the same time, the pre-chamber orifices have been applied in the horizontal direction. Using horizontal-directed orifices on the pre-chamber provides an actual photo of the torch flame and, as a result, a precious flame penetration length as its being detected from the bottom of the CVC. A shadowgraph technique has been used to visualize the premixed flame as it is hard to be visualized by direct photographing due to the lower luminance of the premixed flame. The visualization technique included a transparent bottom of the CVC and a synchronized laser high-speed camera. By observing the torch flame combustion behavior, the influence of the pre-chamber injection hole's specifications on the torch flame's ejection and the combustion in the main chamber, a torch strength index has been proposed in this work.

2. EXPERIMENTAL EQUIPMENT AND TEST PROCEDURES

2.1 Constant Volume Chamber

Table 1 and figure 1 show the main specifications of the constant volume combustion vessel CVC (Constant Volume Chamber). The diameter and height of the applied combustion chamber correspond to the typical medium-speed LBGE. Unlike the actual engine, the main chamber and the pre-chamber do not exchange the ambient during the compression process. This machine is equipped with a special fuel supply system to supply a mixture with different compositions to the pre-chamber and the main chamber. The combustion pressure in both the main chamber and the pre-chamber can be measured, and as a result, the partial pressure between the two chambers can also be indicated. The fuel supply system consists of two mixing systems. A first mixer produces synthetic air from oxygen and nitrogen, and a subsequent mixer provides a CH4/air mixture in the supply system. In the pipeline, pressure regulators and solenoids are installed, and the pulse switching frequency of the solenoid valves is used to control the air/fuel ratio. Using this electronically operated system, the setup can deliver the amount and the required percentages of air and fuel. Figure 5 illustrates the configuration of the fuel supply system.

2.2 The configuration of the PC tip

To study different pre-chambers with various orifices sizes and orifices numbers, different pre-chamber tips have been applied. Then, the experiments were carried out by changing PC tips. PC tip cross-sectional configuration and PC specs are shown in figure 2 and Table 2. The influence of PC design on combustion behavior using five PC tips (#1-#5) was performed. To assess the propagating of the torch flame, PC orifices were created horizontally and positioned at the bottom of the CVC. Tip number #1 is the standard configuration, with an orifice diameter (Dori) of 3.5 mm and 8 orifices (Nori). Tips #2 and #3 have 6 and 10 orifices, respectively, and their total area is nearly identical to that of the #1 tip.

Table 1 Specifications of the CVC

Main chamber (D × H)	∅240 mm × 30 mm
Optical window (D × t)	Quartz ∅260 mm × 100 mm
Max. in-chamber pressure	10 MPa

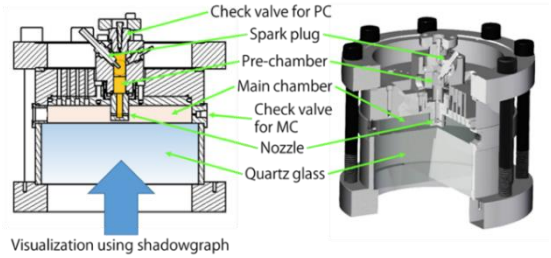

Figure 1. Cross-sectional view of the tested CVC

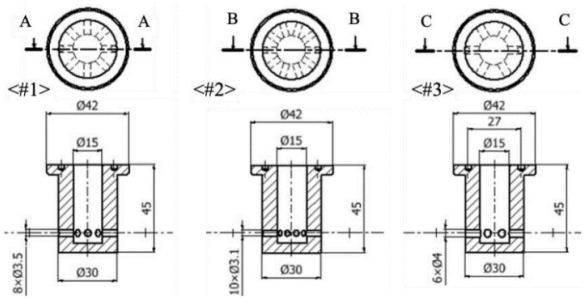

Figure 2. the configuration of the PC tip as a cross-section

2.3 Shadowgraph shooting

Figure 3 shows a pictorial figure of the shadowgraph shooting arrangement, and figure 4 illustrates the outline of the test shadowgraph optical system. A bottom-up reciprocating optical path shadowgraph was applied by using a quartz glass window for the entire bottom surface of the CVC and mirror-finishing the top surface of the inner wall of the container. Figure 4 illustrates the optical setup's orientation and the laser's pathway. Because each ray refracts according to the quadratic spatial gradient of density, the patterns of brighter and darker zones are obtained if the disturbance of the density field induced by premixed flame is present in the measuring volume. The experiment used mirror-polished chamber lids, bottom-up optics layouts, and a half mirror between a shadowgraph illuminator and a high-speed camera to achieve dual-path type shadowgraph optics. To capture shadowgraph photos of the torch flame and combustion process in the MC, a high-speed CMOS camera (Photron Ltd., SA-Z) equipped with a Nikon Teleconverter TC200 2X and Nikon f/2.8 objective lenses were used. An additional high-speed camera (Photron Ltd., SA4) was used to assess the PC's ignition time.

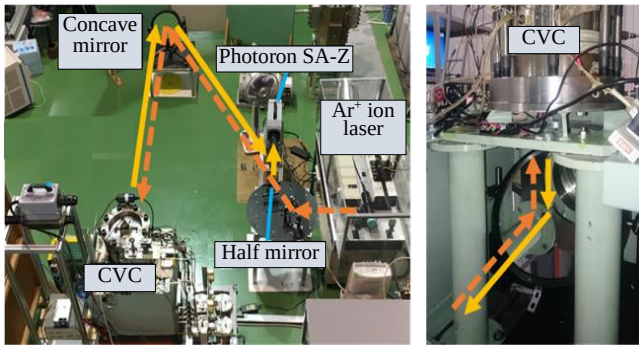

Figure 3. Optical setup of double-path shadowgraph

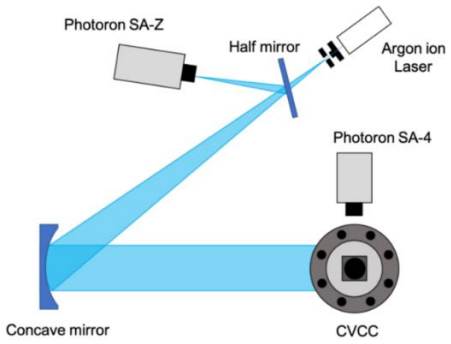

Figure 4. Optical setup of double-path shadowgraph

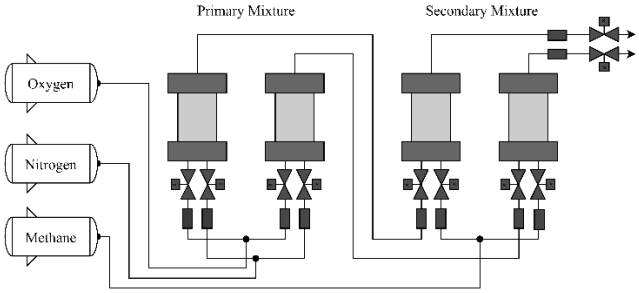

Figure 5. The fuel supply system configuration

Table 2 Specifications of the orifice tips of the pre-chamber

PC tip ID	Hole dia.: Dhole [mm]	Hole length: L_{hole} [mm]	No. of holes: N_{hole} [-]	Tip inner dia.: [mm]	V_{PC}/V_{MC} [%]
#0	∅3.5	7.5	8	∅15	2.3
#1	∅4.0	7.5	6	∅15	2.3
#2	∅3.1	7.5	10	∅15	2.3
#3	∅2.5	7.5	8	∅15	2.3
#4	∅5.0	7.5	8	∅15	2.3
#5	∅3.5	5.0	8	∅10	2.0
#6	∅3.5	7.5	8	∅10	2.0
#7	∅3.5	10.0	8	∅10	2.0
#8	∅3.5	5.0	8	∅20	2.7
#9	∅(3.5/2.2inner)	7.5	8	∅15	2.3

2.4 Specification change of the pre-chamber orifice

Table 2 shows a list of the specifications of the 10 types of pre-chamber orifices tested. The pre-chamber is divided into two parts, and the main body of the pre-chamber equipped with spark plugs and fuel supply valves is common to all experiments. The specifications related to the injection hole can be changed by replacing only the orifice part. However, to measure the reach and spread angle of the torch flame without correction, all the central axes of the injection holes are unified in the horizontal direction. This study studied the ratio between the diameter and length of the injection hole (L/D). Also, the effects of chamber volume and orifice taper have been investigated. In the actual engine (λMC = 1.7), the reaction in the main chamber of the torch flame continues. The standard composition of air (λ MC = ∞) was changed. The premixture supplied to the pre-chamber is based on λ PC = 1.0, and the condition of over-concentration or dilution is also added. Pure methane is used as fuel to eliminate the influence of fuel composition.

3. RESULTS AND DISCUSSION

3.1 Experimental conditions

Figure 6 illustrates an example of torch flame parameters on the shadowgraph observed in the MC. The figure visually shows the penetration and cone angle definition. The penetration length is defined as the distance from the orifice's outlet to the tip of the jet spray. The cone angle is the angle between the jet spray's outward edges from the center of the PC.

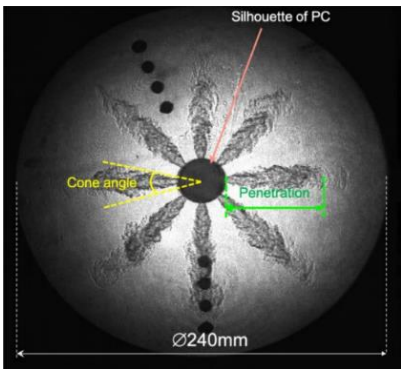

Figure 6. The observed torch flame parameters as an example on the shadowgraph

3.2 Effects of number of holes and diameter of holes

In this section, Visualization and pressure measurements were used to investigate the impact of the PC's number of orifices (Nori) on torch flame and combustion. The number of orifices (Nori) was chosen to be 6, 8, and 10 (tip IDs #1, #2, and #3), respectively. The overall cross-section has been kept the same in all test cases. The 6, 8, and 10 orifices have 4.0 mm, 3.5 mm, and 3.1 mm, respectively. Fig. 7 illustrates the torch flame propagation process in the main chamber when applying different numbers of orifices from 6 to 10. from the figure, decreasing the numbers of the orifices led to an increase in the ejected mixture of Air/Fuel. As a result, the MC combustion process could be enhanced, and the torch flame's penetration and cone angle are both increased. Because the torch flame quickly ignited the previously unburned gas, the penetration differed based on the torch's initial momentum. In the 10-orifice case, the torch flame accelerates as it penetrates further. Figure 8 shows the heat release rate and the accumulated heat

released for a different number of orifices. From the figure, the heat release for both 6 holes and 10 holes seems to be higher than the original case, while the heat release rate was noticed to reach its peak when the number of injection holes is 10. In the premixed phase, in the case of 8 orifices, the released heat has been noticed to be not stable, leading to an increase in the after-burning phase. Also, the lagging in the heat released could be because of the slower combustion propagation in the radial direction.

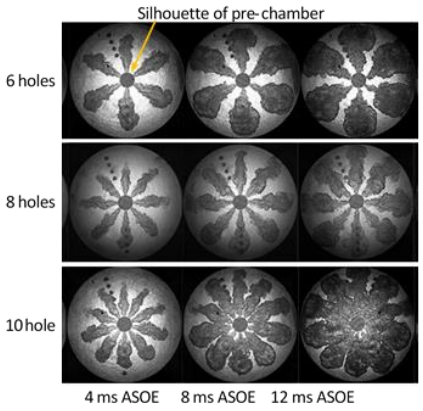

Figure 7. Torch flame penetration process in the main chamber by changing the number of orifice holes from 6 to 10.

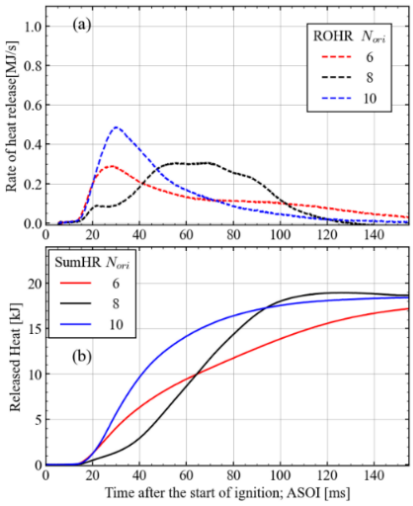

Figure 8. The heat release rate and accumulated released heat in the main chamber by changing the number of orifice holes from 6 to 10.

3.3 Effect of the orifice diameter on the flow path

Figure 9 illustrates the torch flame penetration in the MC using the shadowgraph technique when applying different orifice holes diameter (2.5 mm, 3.5 mm, and 5.0 mm) versus time ASOE. Generally, the torch flame is ejected from the PC to the main chamber in the form of a flammable jet with a different cone angle and propagation speed. The figure noticed that the higher the nozzle diameter, the larger the cone angle. This large cone angle leads to covering a larger area, and in some excessive connecting contours, these stacked flammable jets could be from the ejection's root or the orifices' outlet. In the case of a 2.5 mm orifice, the ignition of the flame started around 4 ms ASOE. Observing the combustion process, the flame is partially combusted even at 8 ms ASOE in contrast with the 3.5 mm case, which started to combust at 4 ms ASOE keeping a thin burning tip. In the case of 5 mm orifice diameter, the flame was flammable before 4 ms ASOE, which made this case able to consume all the charge in the main chamber.

Figure 9 shows the heat release rate and the accumulated heat release in the main chamber for different hole-diameter cases. From the figure, the ejection penetration of the torch flame becomes excessive, and the ignitability of the air-fuel mixture in the main chamber decreases. As the diameter of the orifice increases, the penetration of the torch flame decreases. Applying the orifice diameter ϕ 5.0 mm significantly increased the heat release rate reaching the maximum value among other cases. The maximum value of the heat release rate of the injection hole diameter ϕ 5.0 mm reached almost 1.1MJ/Sec, while this value was less than 0.4 MJ/Sec for both other cases. The figure also shows the start time of the torch flame to be 13 ms for all cases. In the case of the 2.5 mm orifice diameter, the combustion has been noticed to be non-uniform, resulting in extended heat release.

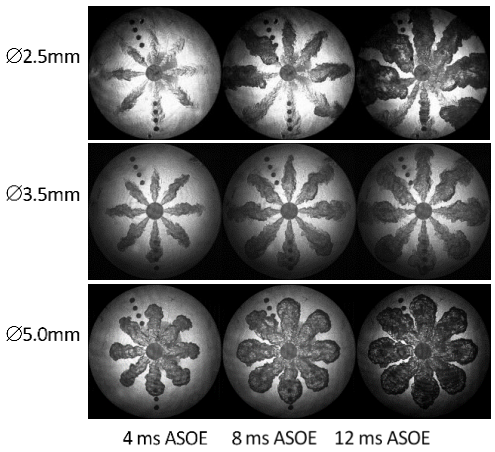

Figure 9. Torch flame penetration process in the MC using different orifice holes diameter ∅2.5 mm, ∅3.5 mm, and ∅5.0 mm.

3.4 Effect of orifice L/D ratio

The diameter and length of the injection hole differ from those of the diesel injector. However, even in the LBGE pre-chamber, the ratio of the injection hole length and the injection hole diameter: (L/D ratio) has been noticed to affect the behavior of the torch flame. Figure 11 shows a shadowgraph of the torch flame ejection process when the L/D ratio of the injection hole is decreased (1.43, # 8) or increased (2.86, # 7) from the reference value (2.14, # 6). The orifice part has been replaced with an inner diameter of ∅ 10 mm at the tip. The ambient in the main chamber is unified to nitrogen (λMC = 0) to evaluate the torch flame's penetration and spread angle. When the L/D ratio is 2.86, the tip of the torch flame at the initial ejection stage has a tapered shape, and it is considered that the ejection speed is excessive under this condition. On the other hand, the penetration force is suppressed at 1.43, which has the minimum L/D ratio. The torch flame base is partially bonded, which is expected to be advantageous for the combustion of the premixed main chamber. Figure 12 shows torch flame penetration and

cone angle versus time for different L/D ratios of the injection hole. The penetration of the torch flame increases as the L/D ratio increases, but even if the L/D ratio is doubled from 1.43 to 2.86, the difference in reach is about 10 mm. On the other hand, the spread angle of the torch flame tends to increase as the L/D ratio decreases, and the difference is significant, especially at the initial ejection stage. It is considered that the cause is that the directivity of the ejection increases as the L/D ratio increases. In addition, the change in the behavior of the torch flame when the injection mentioned above hole diameter was changed included the effect of changing the L/D ratio.

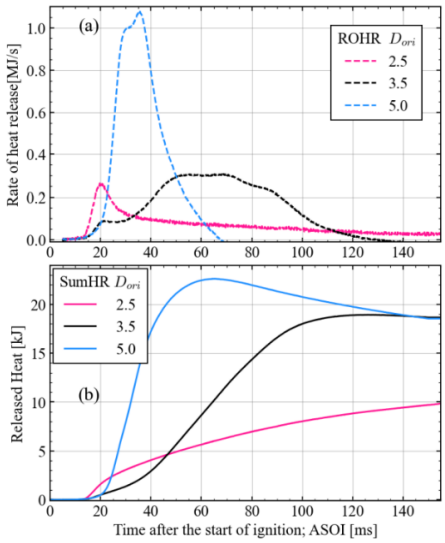

Figure 10. The heat release rate and accumulated heat in the main chamber by changing the orifice hole diameter.

The common injection method in diesel injectors is that the hole of the injector is subjected to an incline that expands toward the outlet to increase the spray spread angle and promote atomization. In the LBGE pre-chamber, the same effect can be expected by providing an inclination in the expansion direction in the injection hole flow path. Figure 13 shows the case where the outlet side injection hole diameter and length are the same as the reference pre-chamber (# 0) (ϕ 3.5 mm, 7.5 mm), and the internal injection hole diameter is reduced to ϕ 2.2 mm and widened. # 9) The shadowgraph of the torch flame in the case of the reference pre-chamber is shown. Due to the widening of the orifice flow path, the torch flame expands in the radial direction as a whole, and it is expected that the ignitability of the air-fuel mixture in the main chamber could be improved. In addition, some connections between torch flames are confirmed.

Figure 13 illustrates the shadowgraph for the torch flame penetration process in the main chamber by changing the channel profile of orifice holes from straight to diverging. A divergent passage has been used with 2.2 to 3.5 mm hole diameter endings. The flame behavior is almost the same for the straight and divergent cases, and its performance was compared to the straight (3.5 mm). The figure shows that the diverging can enhance the penetration at the beginning of the flame ejection yet reach a comparable value to the standard case after the 4 ms ASOE. Figure 13 shows the penetration and the cone angle for the torch flame versus time for the divergent case compared to the straight one. It can be seen that the widening of the orifice flow path has almost no effect on the torch flame penetration, but the spread angle of the torch flame has consistently expanded from the initial stage of injection.

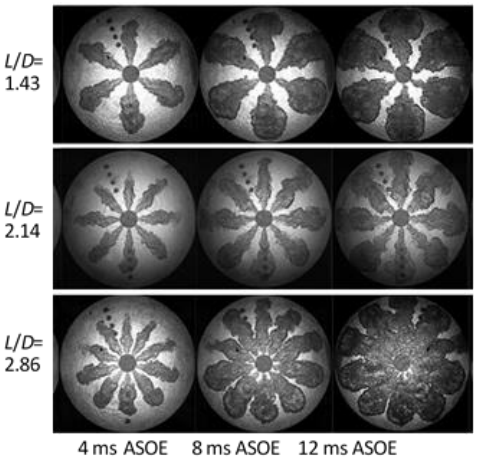

Figure 11. Torch flame penetration process in the main chamber for different L/D ratio orifice holes.

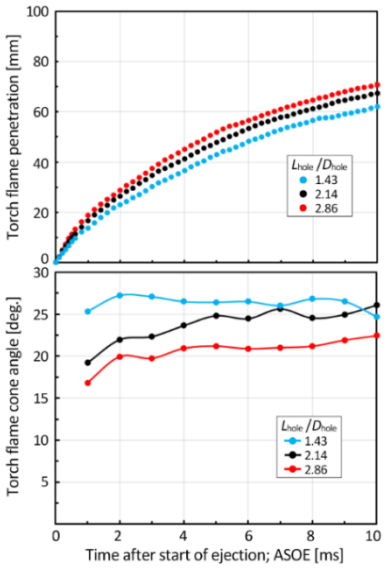

Figure 12. Averaged penetration length and cone angle of torch flames for different L/D ratios of orifice holes

Figure 15 illustrates the torch flame penetration in the MC when applying two different volumes of PC VPC/VMC=2.0% and 2.3%. The penetration of the torch flame is affected by the volume of the PC. This effect could be attributed to the more stored ambient in the pre-chamber, which could increase the torch propagation in the main chamber. Figure 16 shows the torch flame penetration and the cone angle versus time when applying different PC sizes. From the figure, the penetration is proportional to the PC size, in contrast with the cone angle, which decreases by increasing the PC volume with about 5 degrees difference in the cone angle between the two cases.

3.5 Torch strength

From the measurement results, the specifications of the PC and the injection orifice have a significant influence

on the ejection of the torch flame and the combustion in the MC while deteriorating the ignitability of the air-fuel mixture in the main chamber due to the excessive ejection speed of the torch flame is suppressed. However, it is essential to increase the spread of the torch flame and promote the combustion of the air-fuel mixture between the adjacent torch flames. The pre-chamber specifications that affect the ejection strength of the torch flame include the number of holes, the orifice hole diameter, the L/D ratio, the presence or absence of channel expansion, and the pre-chamber-specific volume. The torch strength is calculated based on the relationship between the pre-chamber specs and the combustion behavior in terms of the max injection speed, the flame penetration, the flame cone angle, the combustion period, and the ignition delay. The Torch strength (TS) definition introduced as an index of the ejection intensity of torch flame is as Equ. 1.

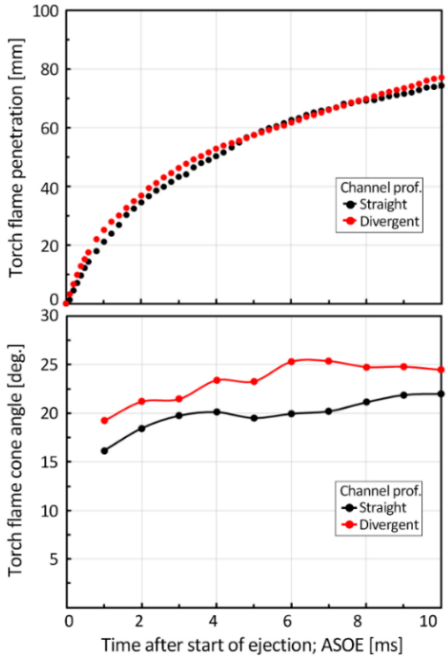

Figure 14. penetration length and cone angle of torch flames changing the channel profile of orifice holes.

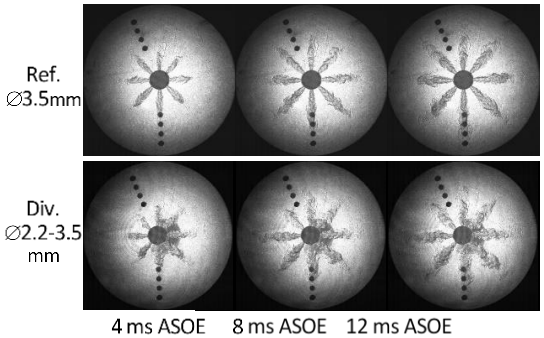

Figure 13 Torch flame penetration process in the main chamber by changing channel profile of orifice holes from straight to diverging.

$$TS \equiv \frac{V_{\mathrm{PC}} \cdot \left({}^{L_{\mathrm{ori}}}/_{D_{\mathrm{ori}}}\right)^{0.5}}{A_{\mathrm{ori}} \cdot N_{\mathrm{ori}}} \ [mm] \qquad (1)$$

V_{PC} is the pre-chamber volume [mm3], L_{ori} is the length of the PC injection orifice [mm], D_{ori} is the diameter of the PC injection hole [mm], A_{ori} is the total area of the PC injection orifices [mm2], N_{ori} represents the number of orifices [-]. The measurement results show that the volume of the main chamber, L/D, is directly proportional to the flame penetration. At the same time, the number of the orifices is reversibly proportional to the flame penetration. Based on these experimental facts, the arrangement of the index has been considered. Also, the power of 0.5 has been chosen to have the best Root-mean-square deviation (RMSD), as shown in Figure 17. First, in order to verify the validity of TS, the Correlation between the TS in all tests pre-chambers and the penetration of the torch flame in the main chamber was considered versus the proposed torch strength since the torch flame penetration is the main measured parameter in this study.

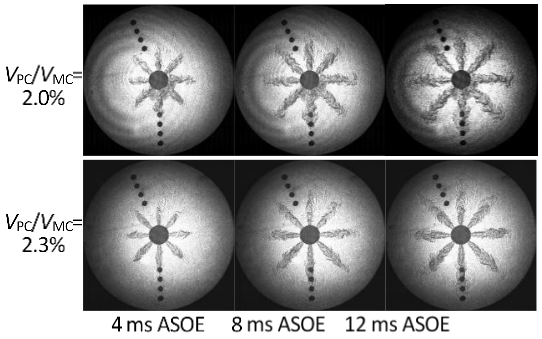

Figure 15. Torch flame penetration in the MC using two different volumes of PC VPC/VMC=2.0% and 2.3%.

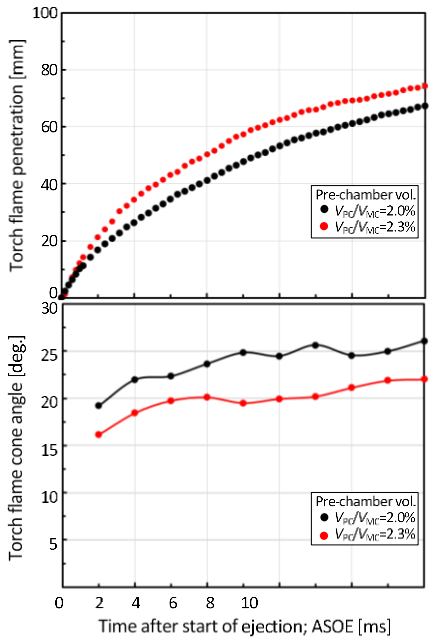

Figure 16. penetration length and cone angle of torch flames by changing pre-chamber volume.

Figure 18 shows the correlation coefficient when the relationship between the TS in the PC and the maximum ejection speed of the torch flame in the main chamber is approximated by a polynomial relation. The Correlation between TS and the maximum ejection velocity has a good overall agreement, indicating that TS is valid as an

index of ejection intensity.

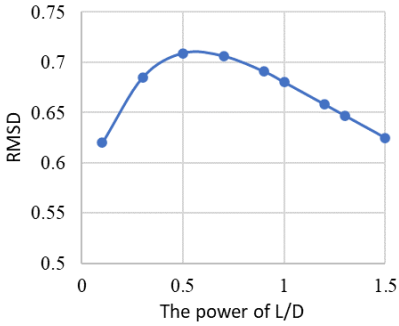

Figure17 Optimizing the power of L/D based on the change in the RMSD.

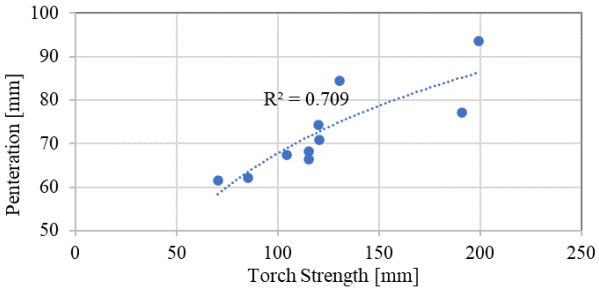

Figure18 TS versus torch flame penetration at 10 ms ASOE.

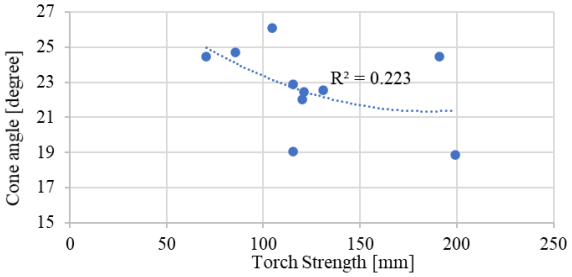

Figure 19 Correlation between TS and cone angle of torch flames at 10 ms ASOE observed in tested pre-chambers.

Figure 19 shows the relationship between the TS of all test PCs and the torch flame's cone angle at 10 ms after the torch flame ejection. The figure shows that the TS seems not to be not accurate for predicting the cone angle. Meanwhile, there is a better agreement in the other combustion parameters, including the combustion duration and max. Injection speed and ignition delay have been noticed. It is worth clarifying that all parameters in the vertical column are measured. The penetration and the cone angle were measured directly from the shadowgraph results. At the same time, the max injection speed was calculated based on the propagation speed of the flame from the penetration measurements. Also, the ignition delay is when the maximum combustion pressure reaches the 5% pressure value from the ignition timing. Finally, the combustion period was assumed to be from the ignition delay to the maximum combustion pressure. Figure 20 shows the correlations between the measured values versus the TS. From the figure, the results have an agreement between the proposed index and the measured values.

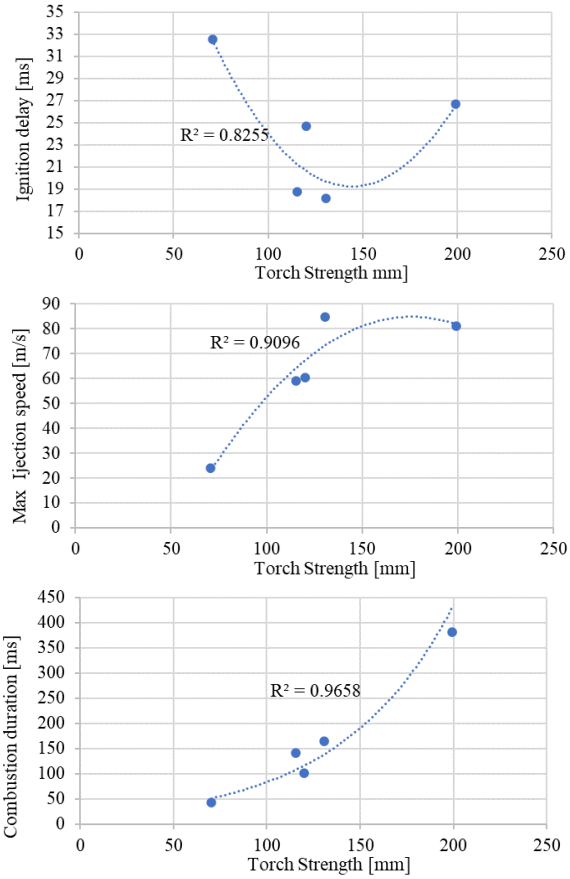

Figure 20 Correlation between TS and penetration/cone angle of torch flames at 10 ms ASOE observed in tested pre-chambers.

4. CONCLUSION

In this study, the combustion in the constant-volume chamber has been visualized. The CVC imitated the common combustion chamber of a pre-chamber medium-speed gas engine. The study used multiple effects of the injection hole specifications of the pre-chamber on the ejection behavior of the torch flame and the combustion in the main chamber. The results are as follows.

1. The specifications of the number, the diameter, the L/D ratio, and the present expansion of the flow path of the holes in the pre-chamber, besides the specific volume of the pre-chamber, had been noticed to affect the reach and spread angle of the torch flame and the ejection speed into the main chamber.
2. Combustion of the air-fuel mixture in the main chamber proceeds mainly by the radial growth of the torch flame. To promote combustion, it is vital to quickly transmit the flame to the gap between the torch flames.
3. When the ejection intensity of the torch flame becomes excessive, the ignition delay of the air-fuel mixture in the main chamber is extended, and the combustion period of the air-fuel mixture in the main chamber tends to be extended. To promote the combustion of the air-fuel mixture in the main chamber, it is essential to increase the spread angle of the torch flame and suppress the excessive ejection speed.

4. By introducing an index of the ejection intensity of the torch flame based on the specifications of the injection hole in the pre-chamber, the measured ejection velocity, reach distance, and spread angle of the torch flame could be described using the proposed Correlation.

5. REFERENCES

[1] (2022) The Intergovernmental Panel on Climate Change [Internet]. 2022,.

[2] (2022) United States Environmental Protection Agency [Internet]. 2022,.

[3] Motaz Mabrouk Salama, Elsihy, E., Moneib, H. et al. The Combustion of a Diesel Oil-Based/Coal/Water Slurry in a Horizontal Cylindrical Furnace: An Experimental Investigation. *Proceedings of International Exchange and Innovation Conference on Engineering & Sciences (IEICES)*, 2021, **7**, 64–70. https://doi.org/10.5109/4738568

[4] Mahmudul, H.M., Hagos, F.Y., Mamat, R. et al. Production, characterization and performance of biodiesel as an alternative fuel in diesel engines – A review. *Renewable and Sustainable Energy Reviews*, Elsevier Ltd. 2017, **72**, 497–509. https://doi.org/10.1016/j.rser.2017.01.001

[5] Lu, T., Lu, Z., Shi, L. et al. Improving the fuel/air mixing and combustion process in a low-speed two-stroke engine by the IFA strategy under EGR atmosphere. *Fuel*, Elsevier Ltd. 2021, **302**, 121200. https://doi.org/10.1016/j.fuel.2021.121200

[6] Nguyen, H.P., Hoang, A.T., Nizetic, S. et al. The electric propulsion system as a green solution for management strategy of CO_2 emission in ocean shipping: A comprehensive review. *International Transactions on Electrical Energy Systems*, 2021, **31**, 1–29. https://doi.org/10.1002/2050-7038.12580

[7] Wei, H., Chen, X., Wang, G. et al. Effect of swirl flow on spray and combustion characteristics with heavy fuel oil under two-stroke marine engine relevant conditions. *Applied Thermal Engineering*, Elsevier Ltd. 2017, **124**, 302–14. https://doi.org/10.1016/j.applthermaleng.2017.05.202

[8] Emission Standards, d. Internal: IMO marine engine regulations [Internet].

[9] Abdelhameed, E., Aoyagi, T., Tashima, H. et al. PIV measurements of entrainment process of directly injected media in internal combustion engines. *14th International Symposium on Particle Image Velocimetry*, 2021, **1**, 1–10. https://doi.org/10.18409/ispiv.v1i1.184

[10] Elsharkawy, E.A. Effect of several types of bio-diesels and their mixtures on the combustion, performance, and emission characteristics of DI diesel engine. *Energy Sources, Part A: Recovery, Utilization and Environmental Effects*, Taylor & Francis. 2020, **00**, 1–15. https://doi.org/10.1080/15567036.2020.1785589

[11] Elsharkawy, E.A., Abou Al-sood, M.M., El-Fakharany, M.K. et al. Assessing and Comparing the Characteristics of CI Engine Powered by Biodiesel–Diesel and Biodiesel–Kerosene Blends. *Arabian Journal for Science and Engineering*, Springer Berlin Heidelberg. 2021, **46**, 11771–82. https://doi.org/10.1007/s13369-021-05703-7

[12] Elsharkawy, E.A., Abou Al-Sood, M.M., El-Fakharany, M.K. et al. Enhancing the Impact of Biodiesel Blend on Combustion, Emissions, and Performance of DI Diesel Engine. *Arabian Journal for Science and Engineering*, Springer Berlin Heidelberg. 2020, **45**, 1109–23. https://doi.org/10.1007/s13369-019-04245-3

[13] Elsharkawy, E.A., Abou Al-Sood, M.M., El-Fakharany, M.K. et al. Comparative study of combustion, performance, and emissions of a diesel engine fuelled with biodiesel blend with metallic and organic nano-particles. *International Journal of Global Warming*, 2020, **22**, 133–59. https://doi.org/10.1504/IJGW.2020.110292

[14] Abdelhameed, E. and Tashima, H. Experimental investigation on methane inert gas dilution effect on marine gas diesel engine performance and emissions. *Energy Sources, Part A: Recovery, Utilization and Environmental Effects*, 2022, **44**, 3584–96.

[15] Zhang, Z., Li, X., Liu, L. et al. Influence of mulched drip irrigation on landscape scale evapotranspiration from farmland in an arid area. *Agricultural Water Management*, Elsevier. 2020, **230**, 105953. https://doi.org/10.1016/j.agwat.2019.105953

[16] Imhof, D., Tsuru, D., Tajima, H. et al. (2013) High-pressure natural gas injection (GI) marine engine research with a Rapid Compression Expansion Machine. *CIMAC Congress 2013*, Shanghai. 2013, p. 11.

[17] Wang, S., Li, Y., Fu, J. et al. Quantitative investigation of the effects of EGR strategies on performance, cycle-to-cycle variations and emissions characteristics of a higher compression ratio and heavy-duty NGSI engine fueled with 99% methane content. *Fuel*, Elsevier. 2020, **263**, 116736. https://doi.org/10.1016/j.fuel.2019.116736

[18] Zhang, Q., Yang, Y., Jia, D. et al. Knocking characteristics of a high pressure direct injection natural gas engine operating in stratified combustion mode. *Open Physics*, 2021, **19**, 534–8. https://doi.org/10.1515/phys-2021-0064

[19] da Costa, R.B.R., Rodrigues Filho, F.A., Moreira, T.A.A. et al. Exploring the lean limit operation and fuel consumption improvement of a homogeneous charge pre-chamber torch ignition system in an SI engine fueled with a gasoline-bioethanol blend. *Energy*, 2020, **197**. https://doi.org/10.1016/j.energy.2020.117300

[20] Zhu, S., Akehurst, S., Lewis, A. et al. A review of the pre-chamber ignition system applied on future low-carbon spark ignition engines. *Renewable and Sustainable Energy Reviews*, Elsevier Ltd. 2022, **154**, 111872. https://doi.org/10.1016/j.rser.2021.111872

[21] Talei, M., Jafarmadar, S. and Khalilarya, S. Experimental and numerical analyses of cold EGR effect on combustion, performance and emissions of natural gas lean-burn engine with pre-chamber combustion system. *Fuel*, Elsevier. 2020, **276**, 118061. https://doi.org/10.1016/j.fuel.2020.118061.